

Impact of Reflectors and MIMO on ML-Aided mmWave/sub-THz Blockage Prediction

Roghieh Mahdavihaji[†], Alexandra Duel-Hallen[†], Hans Hallen[‡]

Department of Electrical and Computer Engineering, North Carolina State University, Raleigh, NC, USA[†]

Physics Department, North Carolina State University, Raleigh, NC, USA[‡]

Emails:{rmahdav2, sasha, hallen}@ncsu.edu

Abstract—The performance of millimeter-wave (mmWave) and sub-terahertz (sub-THz) communication systems is significantly impaired by sensitivity to sudden blockages. In this work, we employ machine learning (ML) and our physics-based simulation tool to warn about the upcoming blockage tens of 5G frames ahead for highway speeds, providing a sufficient time for a proactive response. Performance of this ML-aided early-warning-of-blockage (ML-EW) algorithm is analyzed for realistic outdoor mobile environments with diverse reflectors and antenna arrays placed at the base station (BS) and user equipment (UE) over a range of mmWave and sub-THz frequencies. ML accuracy of about 90% or higher is demonstrated for highway UE, blocker, and reflector speeds, multiple-input-multiple-output (MIMO) systems, and frequencies in mmWave/sub-THz range.

Index Terms—mmWave, sub-THz, blockage prediction, channel modeling, machine learning, Fresnel diffraction, MIMO, reflectors.

I. INTRODUCTION

Utilization of millimeter wave (mmWave) and sub-THz frequencies can potentially boost the throughput of wireless communication systems since they provide much wider available bandwidth than the sub-6 GHz frequencies. However, there are inherent challenges to effective deployment of mmWave/sub-THz technology. In particular, line-of-sight (LoS) blockage by static or moving physical objects can severely limit performance of these systems [1], [2] due to more abrupt variation of the received signal strength (RSS) caused by weaker diffraction and greater penetration loss than for sub-6GHz frequencies [3].

In [8], we employed the MiniRocket Machine Learning (ML) time-series classifier method [4] to provide early warning (EW) of LoS mmWave blockage hundreds of ms ahead for highway speeds using in-band signal observations, thus enabling a proactive response to an upcoming blockage, e.g., a base station (BS) or beam switching. The mmWave signal datasets for training and testing the ML method [8] were created using our low-complexity physics-based simulation tool, which models diffraction accurately [5], [7], [8]. Our insights and numerical results suggest that the proposed early warning method is caused by the diffraction-induced pre-blockage signal patterns. However, [8] did not investigate the impacts of the reflector's sizes and angles, multiple-input-multiple-output (MIMO) antennas, and various carrier

frequencies on the EW performance. In this work, we include the latter features into the ML training and testing data sets for multiple mmWave and sub-THz frequencies and validate the ML-aided EW of blockage capability in these realistic mobile wireless scenarios.

Related work: Below we summarize the works on mobile mmWave blockage prediction that are closely related to this paper's topic since they include either physical modeling or multiple antennas, complementing more comprehensive literature reviews in [8] and other works. In [7], LoS blockage was forecasted based on sub-6 GHz observations using our realistic physical model. While [7] included frequency-dependent diffraction effects associated with reflectors, it did not study the impact of reflectors in the environment on LoS blockage. Fresnel-Kirchhoff diffraction modeling was employed in [9] to detect amplitude fluctuations and diffraction fringe characteristics of low-frequency signals, which were used to warn about upcoming blockage of mmWave signals. In [12], in-band mmWave measurements were employed in recursive neural networks (RNN) and convolutional neural networks (CNN) methods for predicting upcoming LoS blockage using 16-element antenna array at the base station (BS) and a static user equipment (UE) with an omnidirectional antenna in the proximity of a moving blockage. The user's signal strength was used in deep neural networks (DNN) and Long Short-Term Memory (LSTM) algorithms to predict LoS blockage for 3.5 GHz, 30 GHz, and 60 GHz in the system with static BS and UE with 64 and 16 antennas, respectively, and a mobile blocker [13]. In [14], deep learning with adaptive beamforming at BS and a single antenna at UE is employed to predict LoS blockage and initiate a proactive hand-off for a mobile UE system.

Unlike most works in the literature, this paper does not assume specific topology, directions, or speeds and does not use simplistic simulation models. Moreover, our approach relies solely on in-band mmWave or sub-THz signal measurements and does not require sub-6 GHz observation or cameras. Furthermore, we employ the MiniRocket [4] method that is less complex and much faster than deep learning (DL) and RNN models [8]. Finally, the impacts of reflectors in the environment, MIMO configurations, and sub-THz frequencies on the EW of LoS blockage have not been investigated previously.

The rest of the paper is organized as follows. A physics-

This work was partially supported by National Science Foundation Grant ECCS-2122012.

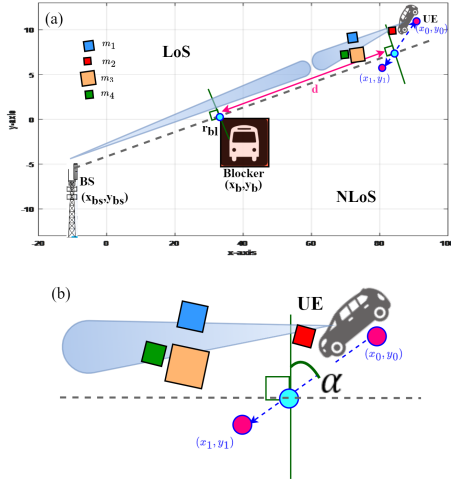


Fig. 1. Example simulation scenario for the physical model; (a) scenario with $Q = 4$ significant reflectors; (b) zoom-in of upper right corner of (a) and rotated so LoS/NLoS edge (dashed line) is horizontal rather than x-axis in (a).

based model is summarized in Section II, highlighting the oscillation patterns associated with LoS blockages and reflectors. The ML method for early warning of blockage is presented in Section III. Section IV contains simulation results for ML-EW algorithm and discusses the impacts of reflectors in the environment, MIMO and the carrier frequency on the RSS and EW accuracy. Finally, conclusions are presented in Section V.

II. PHYSICAL CHANNEL MODEL

The physical model used in this paper is based on the method of images and Fresnel diffraction as detailed in [5], [7], [8]. A 2 dimensional model (2D) is used in this work since a 3D is more complex but unlikely to result in qualitative differences [16]. As in [8], we employ the model to simulate diverse LoS to Non-LoS(NLoS) transitions as well as scenarios without blockage to create the training and testing datasets for the ML-EW method. However, in contrast to [8], this paper considers the presence of both static and moving reflectors with varying sizes. Furthermore, the BS and UE are equipped with linear antenna arrays instead of the omnidirectional antennas assumed in [8]. Fig. 1 depicts an example of the physical model scenario with stationary BS at (x_{bs}, y_{bs}) and blocker (e.g., a parked bus) at (x_b, y_b) implemented as an edge for diffraction in the physical model [7]. The UE is initially positioned at (x_0, y_0) in the LoS region and then moves with constant speed v on a straight line to (x_1, y_1) in the NLoS region. Moreover, Fig. 1 shows $Q = 4$ significant reflectors affecting the received signals as detailed below.

We employ uniform linear arrays (ULA) with L antennas in BS and M antennas in UE. Assume carrier frequency f_k . The phase shifts that must be applied to the transmit and receive antennas in order to point the beams toward azimuth angles θ_t and θ_r relative to the endfire directions, the axes of the arrays, are given by the corresponding steering vectors [15]

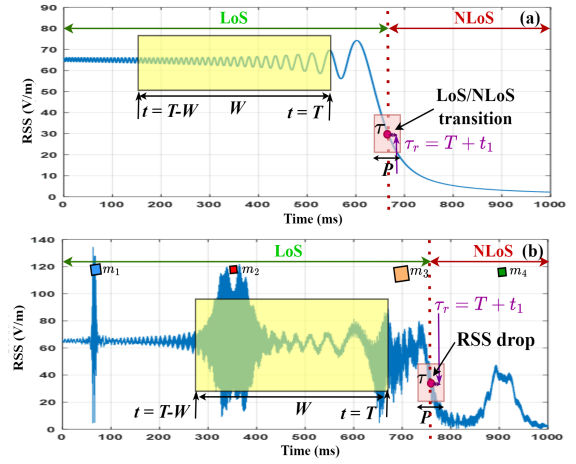


Fig. 2. RSS $|h'_k(t)|$ (3) along the UE path from (x_0, y_0) to (x_1, y_1) in Fig. 1. (a) without reflectors $Q = 0$; (b) with $Q = 4$ stationary reflectors; sizes and angles: m_1 : 0.98 m, 95° ; m_2 : 0.7 m, 95° ; m_3 : 1.5 m, 98° ; m_4 : 0.78 m, 96.4° . Examples of the observation window of length W (ms), prediction window of length P (ms), and other ML-EW parameters are shown; $f_k = 30$ GHz, UE speed $v = 8$ m/s, MIMO $L = 16$ and $M = 4$.

$$\mathbf{a}_t(\theta_t) = [1 \quad e^{j\frac{2\pi\Delta_t \cos \theta_t}{\lambda_k}} \quad \dots \quad e^{j\frac{2\pi(L-1)\Delta_t \cos \theta_t}{\lambda_k}}]_T \quad (1)$$

$$\mathbf{a}_r(\theta_r) = [1 \quad e^{j\frac{2\pi\Delta_r \cos \theta_r}{\lambda_k}} \quad \dots \quad e^{j\frac{2\pi(M-1)\Delta_r \cos \theta_r}{\lambda_k}}]_T \quad (2)$$

where λ_k is the wavelength for frequency f_k and Δ_t and Δ_r are the distances between two adjacent antenna elements of the transmitter (Tx) and receiver (Rx) antennas, respectively. Suppose there are Q significant reflectors ($q = 1, \dots, Q$), i.e., the reflectors within main or side lobes of the Tx and Rx antennas for at least some portion of the UE trajectory. Assuming narrowband transmission (flat fading), the equivalent lowpass gain of the channel from the first element of the transmitter antenna to the first element of receiver antenna, which correspond to the first elements of the steering vectors (1, 2), is given by $h_{k,q}(t)$ for the q^{th} multipath component (MPC). The 'direct', or non-reflected, MPC is represented by the $q = 0$ value, $h_{k,0}(t)$. In these frequency-dependent gains, we account for the diffraction effects as described in eq. (2) of [7]. The equivalent lowpass gain of the channel at frequency f_k that incorporates antenna arrays is given by

$$h'_k(t) = \mathbf{V}_r^T(\theta_{r,q}) \left(\sum_{q=0}^Q h_{k,q}(t) \mathbf{a}_r(\theta_{r,q}) \mathbf{a}_t^T(\theta_{t,q}) \right) \mathbf{V}_t(\theta_{t,q}) \quad (3)$$

where T is the conjugate transpose operator and $\theta_{t,q}$ and $\theta_{r,q}$ are the angles of departure and arrival of the q^{th} path. In (3), we assume that the antennas are optimally aligned for the LoS signal, so the $L \times 1$ and $M \times 1$ unit-magnitude beamforming vectors at BS and UE, respectively, are computed as [15]

$$\mathbf{V}_t(\theta_{t,0}) = \frac{1}{\sqrt{L}} [1 \quad e^{j\frac{2\pi\Delta_t \cos \theta_{t,0}}{\lambda_k}} \quad \dots \quad e^{j\frac{2\pi(L-1)\Delta_t \cos \theta_{t,0}}{\lambda_k}}]_T \quad (4)$$

$$\mathbf{V}_r(\theta_{r,0}) = \frac{1}{\sqrt{M}} [1 \quad e^{j\frac{2\pi\Delta_r \cos \theta_{r,0}}{\lambda_k}} \quad \dots \quad e^{j\frac{2\pi(M-1)\Delta_r \cos \theta_{r,0}}{\lambda_k}}]_T \quad (5)$$

In Fig. 2, we illustrate the downlink $|h'_k(t)|$ for the scenario of Fig. 1. Fig. 2(a) shows diffraction-induced oscillation patterns in the absence of reflectors in the environment. In the LoS region, preceding the geometric LoS/NLoS transition at 680 ms , the oscillations tend to grow in amplitude and decrease in frequency. These patterns are calculated using Fresnel diffraction in the physical model [8]. As discussed in [8], the attributes of the oscillation patterns depend on the carrier frequency, the distance d of the UE path from the blocker edge, angle α from normal at which the UE path crosses the geometric transition line, see Fig. 1(b), and mobile speed. These oscillation patterns occur tens of 5G frames prior to the RSS drop caused by blockage for highway speeds [8]. Fig. 2(b) depicts the RSS $|h'_k(t)|$ (3) affected by the 4 reflectors shown in Fig. 1. Both multipath fading and diffraction-induced oscillations are observed in Fig. 2, but the former have higher frequency than the latter [8]. Due to narrow antenna beams, only one reflector at a time affects the RSS (3). Thus, multipath fading occurs over the region in which both the reflector and LoS paths are present in the antenna lobes, such as a short reflection m_1 near 80 ms , a longer reflection m_2 from $270\text{--}420\text{ ms}$, and m_3 that extends the RSS drop, actively reflecting into the interval $640\text{--}760\text{ ms}$. The relative strengths of the signals on the two paths determine the amplitude of the envelope of the fading. Moreover, in the $890\text{--}930\text{ ms}$ interval, the reflection m_4 occurs in the NLoS region, dominating the multipath signal created by its interference with the remnant, diffracted LoS near the transition. Finally, consistently with the derivations in [7], [8], diffraction-induced oscillations occur when the reflection starts and prior to its end (just inside the reflector edges), changing the multipath fading RSS. In summary, the above reflector effects and antenna models were not included [8] and provide more realistic characterization of mmWave/sub-THz channels necessary for development of accurate ML-EW methods.

III. ML-EW OF BLOCKAGE FOR REALISTIC MIMO SYSTEMS

The MiniRocket classifier is utilized to extract features from the time-correlated samples of $|h'_k(t)|$ (3). It employs (10,000) convolutional kernels of length 12 with random weights and dilation to identify the diffraction-induced features that warn about approaching blockages and to distinguish them from other signal features. Due to the utilization of numerous convolutional kernels with different dilation and padding, MiniRocket classifier is suitable for extraction of oscillation patterns at various frequencies. Furthermore, a linear classifier model, Ridge classifier [6], is trained by the extracted features to predict occurrence of blockage [8].

Fig. 2(b) shows an example of the parameters that are fixed in each ML-EW algorithm implementation: the length of the observation window W (ms), the prediction range t_1 (ms), the length of the prediction window P (ms), and the sampling rate f_s (Hz). Moreover, Fig. 3 depicts the physical model scenarios \mathcal{X}_i used to generate the training and testing dataset $\mathcal{D} = \{\mathcal{X}_i, \mathcal{L}_i\}$ $i = 1, \dots, N$, where \mathcal{X}_i is the 1 ms -

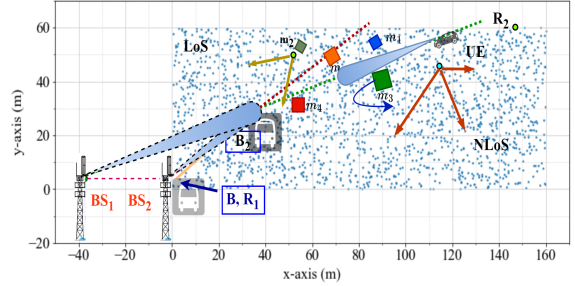


Fig. 3. Physical model configuration to generate dataset \mathcal{D} .

long scenario with specified BS, reflectors, and UE positions, trajectories, speeds, sizes, angles, etc, and \mathcal{L}_i indicates absence ($\mathcal{L}_i = 0$) or presence ($\mathcal{L}_i = 1$) of blockage within the UE trajectory of this \mathcal{X}_i . Given \mathcal{X}_i , if the label $\mathcal{L}_i = 1$, i.e., the trajectory of the UE of this \mathcal{X}_i contains the LoS/NLoS transition, we define the location of the prediction window of length P (ms) as follows. First, we remove all reflectors along the UE trajectory, with the exception of the reflector that extends LoS/NLoS transition if present (e.g., m_3 in Fig. 2(b)). Next, we find the "ground truth" time instance τ where the RSS falls and remains below 50% of the initial LoS RSS value of the UE trajectory, i.e., the UE is in NLoS beyond this point. Note that geometric LoS/NLoS transition (e.g., 680 ms in Fig. 2(a)) occurs at 50% value [7]. Occasionally, a reflection overlaps with the geometric transition and extends the RSS drop, causing a delay in crossing the 50% threshold value (e.g., m_3 causes RSS drop at 760 ms in Fig. 2(b)). Finally, reflectors in LoS (e.g., m_1 and m_2) and in NLoS (e.g., m_4) in Fig. 2(b) can temporarily drop and raise the RSS below or above 50% threshold, respectively. However, those events do not affect the calculation of τ , since we drop such reflectors prior to computing it. Finally, we position τ as the midpoint of the prediction window, which is P (ms) long. Once the prediction window is fixed, we randomly choose a point τ_r (ms) within it, and position the end of the observation window of length W (ms) at $T = \tau_r - t_1$. Finally, if $\mathcal{L}_i = 0$, the location of the prediction window is chosen randomly within UE trajectory.

During training, RSS (3) of the UE trajectory \mathcal{X}_i sampled at rate f_s (Hz) within the observation window of length W (ms) is associated with the predetermined label \mathcal{L}_i . Note that as the length of P (ms) increases, greater variation of the observation window position prior to blockage occurs, thus facilitating improved learning and more accurate prediction as shown in section IV. Finally, when testing, the algorithm observes the samples within the window of length W (ms) of the mobile trajectory (positioned as explained above for datasets with and without blockage) and classifies the corresponding dataset as "blockage" $\hat{\mathcal{L}}_i = 1$ or "absence of blockage" $\hat{\mathcal{L}}_i = 0$. If $\mathcal{L}_i = \hat{\mathcal{L}}_i$, the dataset \mathcal{X}_i is classified correctly.

In Fig. 3, the rectangular shaded region formed by $R_1 = (0, 0)\text{ m}$ and $R_2 = (160, 160)\text{ m}$ is the area in which UE

TABLE I

ML-EW PERFORMANCE vs DATASET SIZE N , $W = 400ms$, $f_s = 1kHz$, $t_1 = 100ms$, $P = 50ms$, $f_k = 30GHz$, $L = 16$, $M = 4$.

N	Accuracy	F1 score	AUC
4000	89.87%	89.86%	89.87%
6000	90.30%	90.29%	90.28%
8000	90.52%	90.51%	90.52%
10000	90.77%	90.77%	90.76%
12000	90.75%	90.75%	90.74%
14000	90.77%	90.76%	90.76%
15000	90.80%	90.81%	90.80%

and blocker trajectories are defined for each scenario. The UE trajectory originates in LoS and terminates in either LoS or NLoS to generate a rich dataset of various scenarios. The blocker starts its movement from point $B = (0,0) m$, and UE starts from a point randomly placed within shaded region shown in Fig. 3. In each scenario, BS is stationary and is placed randomly along the dashed line between $BS_1 = (-40,0) m$ and $BS_2 = (-0.5,0) m$. We create a diverse dataset of scenarios by using independent, uniform distributions to select the directions and speeds of the UE and blocker between 0 and 30 m/s as well as the distances and angles between the UE, the blocker and the BS positions. These variations aim to capture various diffraction-induced patterns and multipath with different rates and amplitudes. The dataset \mathcal{D} is balanced, with 50% of the scenarios labeled as $\mathcal{L}_i = 1$ and the other 50% labeled as $\mathcal{L}_i = 0$. This ensures that the model trained on this dataset will not be biased towards one class.

Moreover, BS and UE are equipped with uniform linear dipole antennas array of sizes L and M , respectively, as described in section II, and variety of sizes, orientations and speeds of the reflectors are employed. The number of dominant reflectors is expected to be small in 5G/6G systems due to utilization of MIMO [3]. In this paper, we only consider reflectors with flat reflecting surfaces as contribution of a curved reflector is much weaker with distance from the reflector [16]. Thus, we define the size of the reflector as its length in 2D, with the position coordinates at the center, and its angle measured from the positive x-axis. To generate each scenario, we position Q significant reflectors randomly using uniform distribution where Q is between 0 and 10. To enhance the computational efficiency without compromising accuracy, we consider only significant reflectors that are within antennas' lobes during UE trajectory. Reflector sizes range from 0.1 m to 2 m while reflectors' angles are randomized using uniform distribution between 0° and 360° . For scenarios with $Q \geq 8$, we randomly choose either one or two moving or rotating reflectors as follows: a reflector moves with speed that varies randomly between 0 and 30 m/s (e.g., reflector m_2 in Fig. 3) or rotates with randomly chosen initial and final angles between 0° and 360° from positive x-axis (e.g., reflector m_3 in Fig. 3).

Finally, to test the effectiveness of the ML-based early warning method, we use k-fold cross-validation with $k = 5$. The dataset is randomly split into 5 groups, \mathcal{D}_1 to \mathcal{D}_5 . The model is trained on four groups at a time and tested on the

TABLE II

ML-EW PERFORMANCE vs SAMPLING FREQUENCY f_s , $N = 10000$, $W = 400ms$, $t_1 = 100ms$, $P = 50ms$, $f_k = 30GHz$, $L = 16$, $M = 4$.

f_s (Hz)	Accuracy	F1 score	AUC
1000	90.77%	90.76%	90.74%
2000	91.39%	91.38%	91.38%
3000	91.63%	91.62%	91.62%
4000	92.32%	92.31%	92.31%
5000	92.24%	92.23%	92.23%

TABLE III

ML-EW PERFORMANCE vs PREDICTION RANGE t_1 AND INTERVAL P , $W = 400ms$, $f_s = 4kHz$, $M = 4$, $L = 16$, $f_k = 30GHz$.

P (ms)	t_1 (ms)	Accuracy	F1 score	AUC
10	≤ 100	91.86%	91.85%	91.85%
10	150	90.05%	90.04%	90.04%
10	200	88.29%	88.27%	88.27%
10	250	85.67%	85.65%	85.67%
10	350	81.62%	81.61%	81.61%
25	≤ 100	92.22%	92.21%	92.21%
25	150	90.78%	90.77%	90.76%
25	200	88.34%	88.32%	88.32%
25	250	85.74%	85.71%	85.71%
25	350	81.71%	81.70%	81.70%
50	≤ 100	92.32%	92.31%	92.31%
50	150	90.90%	90.89%	90.89%
50	200	88.72%	88.73%	88.70%
50	250	85.81%	85.80%	85.80%
50	350	81.90%	81.90%	81.89%

remaining group to evaluate its predictive performance. This process is repeated five times, so that each group is tested once. To evaluate the performance of our ML-EW method, we use three metrics: accuracy, f_1 score, and area under the curve (AUC) [8]. The accuracy metric measures the percentage of correctly predicted labels while the f_1 score combines both precision and recall to provide an overall measure of the classifier's effectiveness.

IV. NUMERICAL RESULTS

This section evaluates the effectiveness and accuracy of the ML-EW method for MIMO mmWave/sub-THz channels with reflectors in the environment.

A. EW Performance

In this subsection, we fix $f_k = 30 GHz$ and $L = 16$, $M = 4$. The effect of varying these parameters will be examined in the following subsections. In Tables I and II, we compare the

TABLE IV

ML-EW ACCURACY FOR MIMO ($L = 16$, $M = 4$) AND OMNIDIRECTIONAL ANTENNAS, $f_s = 4kHz$, $W = 400ms$, $P = 50ms$, $f_k = 30GHz$.

t_1 (ms)	MIMO ($Q=0$)	MIMO ($Q \leq 10$)	Omnidirectional ($Q \leq 10$)
≤ 100	97.93%	92.32%	88.11%
150	97.38%	90.89%	85.73%
200	96.55%	87.73%	83.52%
250	95.50%	85.67%	80.86%
350	94%	81.90%	77.90%

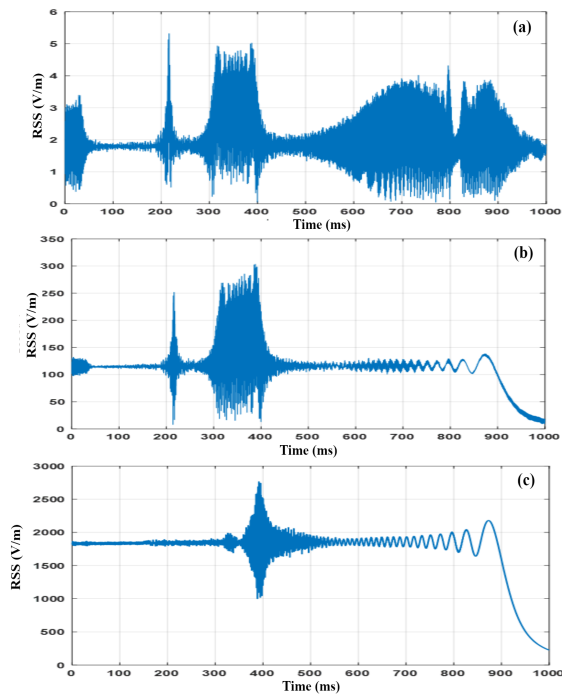


Fig. 4. RSS $|h'_k(t)|$ (3) for the same set of 9 reflectors (a) omnidirectional antennas; (b) MIMO with $M = 4$, $L = 16$; (c) MIMO with $M = 16$, $L = 64$, $f_k = 30\text{GHz}$; UE speed = 17m/s , blocker speed = 9m/s .

accuracy of ML for a varying dataset sizes N and sampling frequencies f_s . As in [8], we found that choosing $W = 400$ m_s provides desirable performance complexity trade-off. From Table I, we note that increasing N to values above 10000 does not significantly improve performance. Moreover, from Table II, ML performance improves as f_s increases and saturates at $f_s = 4$ kHz. Similar conclusions were reached for other MIMO configurations and carrier frequencies. Thus, we choose $N = 10000$, $W = 400$ m_s and $f_s = 4$ kHz in the remainder of this section. Table III shows that performance of ML-EW improves as t_1 decreases and P increases as expected. These results demonstrate that the ML-EW method achieves accuracy of over 90% for $t_1 = 150$ m_s in the reflector-rich environments, corresponding to 15 frames or hundreds of slots in 5G networks. This prediction range is sufficient for a proactive response to the upcoming blockage.

B. Impact of MIMO and Reflectors

In Fig. 4, we compare the RSS of MIMO with that of the omnidirectional antennas with 9 reflectors, where one of the reflectors is moving with speed 2 m/s and one is rotating with initial/final angles ($97^\circ/320^\circ$). Due to the narrower beamwidths of MIMO signals, the impact of reflectors on the RSS is smaller than for omnidirectional antennas. Moreover in reflector-rich environments, the ML-EW performance is enhanced by using larger array sizes since the number of significant reflectors decreases as the antenna size grows.

For each antenna array configuration, the ML-EW algorithm is trained and tested separately. Table IV shows its performance for MIMO and omnidirectional antennas with

TABLE V
ML-EW PERFORMANCE VS ARRAY SIZES L AND M ;
 $f_s = 4\text{KHZ}$, $W = 400\text{ms}$, $t_1 = 100\text{ms}$, $P = 50\text{ms}$ AND
 $f_k = 30\text{GHZ}$.

Array size	Accuracy	F1 score	AUC
$L = 16, M = 4$	92.32%	92.31%	92.31%
$L = 32, M = 4$	93.07%	93.06%	93.06%
$L = 48, M = 4$	93.70%	93.69%	93.69%
$L = 16, M = 8$	93.39%	93.38%	93.38%
$L = 16, M = 16$	94.43%	94.42%	94.42%
$L = 64, M = 16$	96.06%	96.05%	96.05%

TABLE VI
EW PERFORMANCE VS CARRIER FREQUENCY f_k , $L = 16$,
 $M = 4$, $f_s = 4\text{KHZ}$, $W = 400\text{ms}$, $t_1 = 100\text{ms}$, $P = 50\text{ms}$.

f_k (GHz)	Accuracy	F1 score	AUC
30	92.32%	92.31%	92.31%
60	91.96%	91.95%	91.95%
80	91.75%	91.74%	91.74%
100	91.43%	91.42%	91.42%
150	91.21%	91.20%	91.20%
200	90.58%	90.57%	90.57%
250	90.44%	90.43%	90.43%
300	90.32%	90.31%	90.30%

and without reflectors in the environment. We found that performance is similar for MIMO and omnidirectional antennas ($Q = 0$). However, presence of reflectors degrades ML performance due to the additional oscillation patterns and RSS fluctuations as discussed in section II. Furthermore, reflection around LoS/NLoS transition (Fig. 1) can extend strong RSS as shown in Fig. 2(b). Since such events do not affect the observation window, they cannot be predicted in advance with the proposed ML method, thus further reducing its accuracy. However, employing MIMO improves the performance of EW up to 5% in the environments with reflectors ($Q > 0$). Finally, ML-EW results for different array sizes are presented in Table V. With $L = 64$ and $M = 16$, ML-EW achieves the accuracy of 96%, an improvement of about 4% compared to $L = 16$ and $M = 4$.

C. Dependency on the Carrier Frequency

Table VI presents the performance of ML-EW vs the carrier frequency f_k in the mmWave and sub-THz range. For each frequency f_k , the model is trained and tested separately. We observe that the accuracy of ML-EW is above 90% for all frequencies, with slight drop in accuracy as f_k increases. Therefore, ML-EW is suitable for blockage prediction in 5G/6G systems. Furthermore, the derivations in [8] shows that that the diffraction-induced oscillation patterns preceding blockage retain their features but compress in space by a factor of $\sqrt{f_k}$. The effect of f_k on oscillation patterns prior to blockage with and without reflectors is depicted in Fig. 5.

D. Impact of Mobility

In this subsection, we study the effect of UE, blocker and reflector speeds on the EW performance. First, training of ML is performed jointly for all speeds. Next, we split the set \mathcal{D} (see section III) into 9 subsets with the speed of mobile objects restricted to the ranges shown in Table VII.

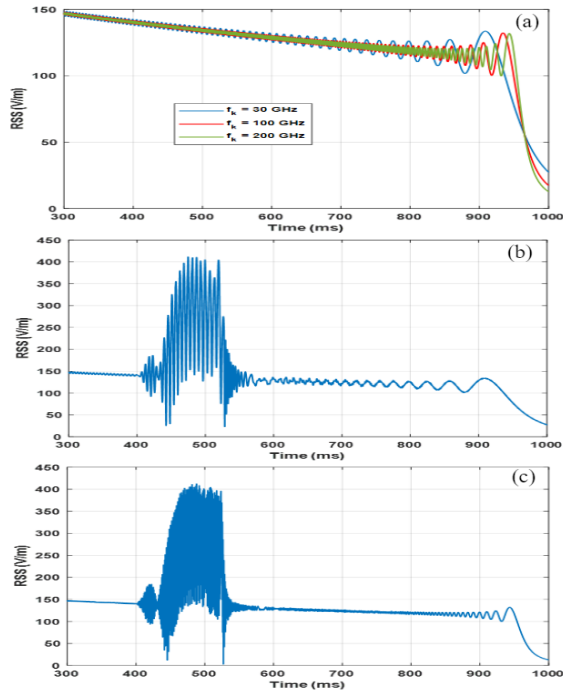


Fig. 5. RSS $|h'_k(t)|$ (3) with $L = 16$ and $M = 4$; (a) in the absence of reflectors ($Q = 0$); (b) $f_k = 30$ GHz and (c) $f_k = 200$ GHz with $Q = 2$ stationary reflectors; UE speed = 23 m/s, blocker speed = 21 m/s

TABLE VII
ML-EW ACCURACY FOR MIMO SYSTEM ($L=16, M=4$) VS
UE AND BLOCKER ($v_{UE,B}$) AND REFLECTOR (v_q)
SPEEDS, $f_s=4$ KHZ, $W = 400$ ms, $t_1 = 100$ ms, $P = 50$ ms,
 $f_k = 30$ GHZ.

$v_q \backslash v_{UE,B}$	0-10	10-20	20-30
0-10	89.01%	90.02%	90.17%
10-20	88.11%	89.22%	90.08%
20-30	87.94%	88.21%	89.50%

To evaluate the effect of the reflector speed on ML-EW, we include two moving reflectors for any Q value. Within a fixed UE/blocker speed subset, we observe that the effect of reflectors on RSS decrease slightly as reflector speed increases and, therefore, the accuracy of ML-EW increases, which can be explained by shorter durations and higher oscillation rates of faster reflectors. On the other hand, within each reflector speed subset, the accuracy of ML-EW decreases slightly as UE/blocker speeds increase. This can be explained by higher rate of diffraction-induced oscillations as UE/blocker speeds grow since pre-blockage oscillation patterns are space-invariant and thus compress in time as mobility increases [8]. However, our results show that EW of blockage is still feasible for highway speeds.

V. CONCLUSION

In this work, we developed and evaluated the performance of ML-based early warning of LoS blockage method for mmWave and sub-THz systems in environments with reflectors and directional antennas at the BS and the UE. The proposed

ML-EW method is trained and tested using our realistic physical model that accurately models the diffraction oscillation patterns associated with reflectors and approaching blockers. We show that the proposed EW method forecasts approaching blockage sufficiently far ahead to enable a proactive response in mobile systems, such as finding a new beam or performing a handover between base stations. In particular, our results indicate that ML-EW performance accuracy approximates or exceeds 90% over the mmWave and sub-THz range (between 30 GHz and 300 GHz) when the range is 100 m ahead at highway speeds.

REFERENCES

- [1] S. Sur, X. Zhang, P. Ramanathan, and R. Chandra, "Beamspy: Enabling robust 60 GHz links under blockage," in 13th USENIX Symposium on Networked Systems Design and Implementation (NSDI 16), 2016, pp. 193–206.
- [2] T. S. Rappaport, Y. Xing, O. Kanhere, S. Ju, A. Madanayake, S. Mandal, A. Alkhateeb, and G. C. Trichopoulos, "Wireless communications and applications above 100 ghz: Opportunities and challenges for 6g and beyond," IEEE Access, vol. 7, pp. 78 729–78 757, 2019.
- [3] T. S. Rappaport, G. R. MacCartney, M. K. Samimi, and S. Sun, "Wide-band millimeter-wave propagation measurements and channel models for future wireless communication system design," IEEE Transactions on Communications, vol. 63, no. 9, pp. 3029–3056, 2015.
- [4] A. Dempster, D. F. Schmidt, and G. I. Webb, "Minirocket: A very fast (almost) deterministic transform for time series classification," in Proceedings of the 27th ACM SIGKDD Conference on Knowledge Discovery & Data Mining, 2021, pp. 248–257.
- [5] H. Hallen, A. Duel-Hallen, S. Hu, T.-S. Yang, and M. Lei, "A physical model for wireless channels to provide insights for long range prediction," in MILCOM. Proceedings, vol. 1. IEEE, 2002, pp. 627–631.
- [6] C. M. Bishop and N. M. Nasrabadi, Pattern Recognition and Machine Learning, vol. 4, no. 4. New York, NY, USA: Springer, 2006.
- [7] Z. Ali, A. Duel-Hallen, and H. Hallen, "Early warning of mmWave signal blockage and AoA transition using sub-6 GHz observations," IEEE Communications Letters, vol. 24, no. 1, pp. 207–211, 2019.
- [8] A. Fallah Dizche, A. Duel-Hallen and H. Hallen, "Early Warning of mmWave Signal Blockage Using Diffraction Properties and Machine Learning," in IEEE Communications Letters, vol. 26, no. 12, pp. 2944–2948, 2022.
- [9] L. Yu, J. Zhang, Y. Zhang, X. Li and G. Liu, "Long-Range Blockage Prediction Based on Diffraction Fringe Characteristics for mmWave Communications," in IEEE Communications Letters, vol. 26, no. 7, pp. 1683–1687, July 2022.
- [10] M. Alrabeiah and A. Alkhateeb, "Deep Learning for mmWave Beam and Blockage Prediction Using Sub-6 GHz Channels," in IEEE Transactions on Communications, vol. 68, no. 9, pp. 5504–5518, Sept. 2020.
- [11] F. Götsch and M. Kaneko, "Deep Learning-based Beamforming and Blockage Prediction for Sub-6GHz/mm Wave Mobile Networks," -IEEE Global Communications Conference, pp. 1-6, 2020.
- [12] S. Wu, M. Alrabeiah, C. Chakrabarti and A. Alkhateeb, "Blockage Prediction Using Wireless Signatures: Deep Learning Enables Real-World Demonstration," in IEEE Open Journal of the Communications Society, vol. 3, pp. 776–796, 2022.
- [13] S. K. Chari and G. P. Koudouridis, "Link Blockage Modelling for Channel State Prediction in Higher Frequencies Using Deep Learning," 10th International Conference on Modern Circuits and Systems Technologies (MOCAST), pp. 1-5, 2021.
- [14] A. Alkhateeb, I. Beltagy, and S. Alex, "Machine learning for reliable mmwave systems: blockage prediction and proactive handoff," in IEEE Global Conference on Signal and Information Processing (GlobalSIP), pp. 1055–1059, 2018.
- [15] R. Heath, A. Lozano, *Foundations of MIMO Communication*. Cambridge: Cambridge University Press, 2018, doi:10.1017/9781139049276.
- [16] Ziad Ali, Alexandra Duel-Hallen, Hans Hallen, November 6, 2019, "Supplementary Material for "Early Warning of mmWave Signal Blockage and AoA Transition Using sub-6 GHz Observations"", IEEE Dataport, doi: <https://dx.doi.org/10.21227/xyrw-mv20>.